Supplementary Information (SI) for Journal of Materials Chemistry A.
This journal is © The Royal Society of Chemistry 2025

Supporting Information for

Molecular anchoring induced charge transfer pathway conversion from p-n to S-scheme heterojunction for boosting photocatalytic hydrogen evolution and N_2 fixation

Xiaoyan Lu, Xinhui Jiang, Jindou Hu*, Junhong Li, Anjie Liu, Zhenjiang Lu, Jing Xie, Yali Cao*

State Key Laboratory of Chemistry and Utilization of Carbon Based Energy Resources, College of Chemistry, Xinjiang University, Urumqi 830017, Xinjiang, PR China.

*Corresponding author.

E-mail address: caoyali523@163.com; hujindu@xju.edu.cn

Evaluation of photocatalytic H_2 evolution performance

The photocatalytic hydrogen evolution test was taken on a sealed system with 100 mg catalyst and 100 mL 25 vol% methanol aqueous solution. Generally, under the magnetic stirring, the catalyst was uniformly suspended in a sealed quartz reactor. The 300 W Xenon lamp was selected as irradiation light, the reactor was placed 15 cm away from the lamp. Prior to the photocatalytic reaction, the system must be thoroughly degassed to a vacuum state to eliminate the interference of air. The integral area of the produced H_2 was recorded by the online detection system of the gas chromatograph (GC 7920) and nitrogen was used as a carrier gas in the conductivity detector (TCD).

Evaluation of photocatalytic N_2 reduction performance

The photocatalytic nitrogen fixation experiments were detected in a sealed reactor with 100 mL of 2.5 vol % methanol solution and 50 mg of catalysts. Before irradiation, purity N_2 (>99.999%) was continuously bubbling in a sealed reactor for 30 min to remove oxygen contaminants and ensure to acquire a nitrogen-saturated solution. Whereafter, 300 W Xe lamp (CEL-HXF300-T3) was used as the simulated light source to illuminate the reactor for 2.5 h at full spectrum. Over the reaction, the 5 mL sample was filtered through a 0.22 μm organic filter membrane to remove the residual solid catalyst. Additionally, the concentration of NH_4^+ produced by the photocatalytic N_2 reduction experiment was detected by Nessler's reagent method.

Photoelectrochemical measurements

The photoelectrodes were prepared on fluorine-doped tin oxide (FTO) glass slides. 5 mg of the prepared samples were added into 100 μL of methanol and then ultrasonic treatment for a short while to form homogeneous slurry. Thereafter, the prepared slurry was uniformly applied to the conductive side of FTO glass and the drop area was kept at 2 cm^{-2}. After drying at room temperature, the photoelectrochemical responses of the obtained electrodes were tested in a typical three-electrode system by electrochemical workstation CHI 760 (Shanghai Chen Hua).

During the test process, the prepared electrode, Pt wire, and Ag/AgCl electrode served as the working, counter, and reference electrode, respectively. The electrolyte was prepared with 0.5 M Na_2SO_4 aqueous solution. In this system, the transient photocurrent responses were tested using the amperometric (i-t curves) technique under 300 W Xe light irradiation. LSV test was performed to evaluate the photocatalytic activity of the prepared catalyst. Electrochemical impedance spectroscopy of the catalyst was tested under light and dark conditions to evaluate the photoelectrochemical properties.

Instrumentation

The morphology and structure of the fabricated samples were characterized by field emission scanning electron microscope (FESEM, Hitachi S-4800H), transmission electron microscope (TEM and HRTEM, FEI Tecnai G2F20), selected area electron diffraction (SAED) and high-angle annular dark-field scanning transmission electron microscopy (HAADF–STEM, FEI Themis Z). The composition of samples was determined by Energy Dispersive Spectrometer (EDS), Fourier transform infrared spectroscopy (FTIR, Bruker VERTEX 70), Raman spectroscope (Renishaw Micro-Raman), and X-ray diffractometer (XRD, Bruker D8 Advance, Cu Kα). The loading mass of Cu cocatalyst was detected by inductively coupled plasma optical emission spectrometry (ICP-OES, Optima 8000). The chemical composition and valence states of the samples were analyzed by X-ray photoelectron spectroscopy (XPS, Thermo Fisher Scientiffc ESCALAB250Xi). UV–Vis absorption spectra were measured by Hitachi U-3900H spectrophotometer. The ability of the species to separate photo-generated electron-hole pairs was tested on steady-state fluorescence spectrometer (F-4500, Hitachi, Japan). The carrier lifetime of the as-prepared species were tested on transient fluorescence spectrometer (Edinburgh FLS-1000). Unpaired electrons were examined by electron paramagnetic resonance (EPR, Bruker EMX nano) spectroscopy. The surface photovoltage spectroscopy (SPS) response of catalyst was detected by a surface photovoltage system (CEL-SPS1000). Recorded the Nitrogen adsorption/desorption isotherms on Quantachrome autosorb IQ to determine

the specific surface area, pore size and pore volume of catalysts, which were calculated based on Brunauer-Emmett-Teller (BET) method.

The concentration and rate of NH_4^+ produced by photocatalytic N_2 reduction reaction

It can be seen from the experiment that the standard curve equation is (y=0.2155x-0.0048, R^2=0.9994). In order to compare with the literature, the unit of NH_4^+ concentration is converted from mg/L to μmol/g, according to the formula.

$$n=\frac{C\left(NH_4^+\right)\times V}{18\times m_{cat.}}\times 1000$$

where n is the amount of nitrogen fixation at time t in μmol g^{-1} and c in mg L^{-1}; 18 corresponds to the molar mass of NH_4^+ in g/mol. V is the initial volume of the solution, which is 0.1 L in this paper, and m is the initial mass of catalyst added, which is 0.05 g in this paper, respectively.

Calculation

The load of metal copper:

$M_{CuCl_2\cdot 2H_2O}$=170.48 g/mol M_{TiO_2}=79.87 g/mol

$$n_{TiO_2}=\frac{m}{M}=\frac{0.5g}{79.87\frac{g}{mol}}=0.00626\,mol$$

$$\omega(Cu)=\frac{n_{CuCl_2\cdot 2H_2O}}{n_{TiO_2}+n_{CuCl_2\cdot 2H_2O}}\times 100\%=0.5\%$$

$n_{CuCl_2\cdot 2H_2O}$=0.0000313 mol

$M_{CuCl_2\cdot 2H_2O}=170.48$ g/mol

$m_{CuCl_2\cdot 2H_2O}=n_{CuCl_2\cdot 2H_2O}\times M_{CuCl_2\cdot 2H_2O}$=0.0000313 × 170.48 g/mol=0.0053 g

$$\omega(Cu)=\frac{n_{CuCl_2\cdot 2H_2O}}{n_{TiO_2}+n_{CuCl_2\cdot 2H_2O}}\times 100\% =1.0\%$$

$n_{CuCl_2\cdot 2H_2O}$=0.0000586 mol

$m_{CuCl_2\cdot 2H_2O}=n_{CuCl_2\cdot 2H_2O}\times M_{CuCl_2\cdot 2H_2O}$=0.01 g

$$\omega(Cu)=\frac{n_{CuCl_2\cdot 2H_2O}}{n_{TiO_2}+n_{CuCl_2\cdot 2H_2O}}\times 100\% =1.5\%$$ $n_{CuCl_2\cdot 2H_2O}$=0.0000938 mol

$m_{CuCl_2\cdot 2H_2O}=n_{CuCl_2\cdot 2H_2O}\times M_{CuCl_2\cdot 2H_2O}$=0.016 g

$$\omega(Cu)=\frac{n_{CuCl_2\cdot 2H_2O}}{n_{TiO_2}+n_{CuCl_2\cdot 2H_2O}}\times 100\% =2.0\%$$ $n_{CuCl_2\cdot 2H_2O}$=0.000125 mol

$m_{CuCl_2\cdot 2H_2O}=n_{CuCl_2\cdot 2H_2O}\times M_{CuCl_2\cdot 2H_2O}$=0.0213 g

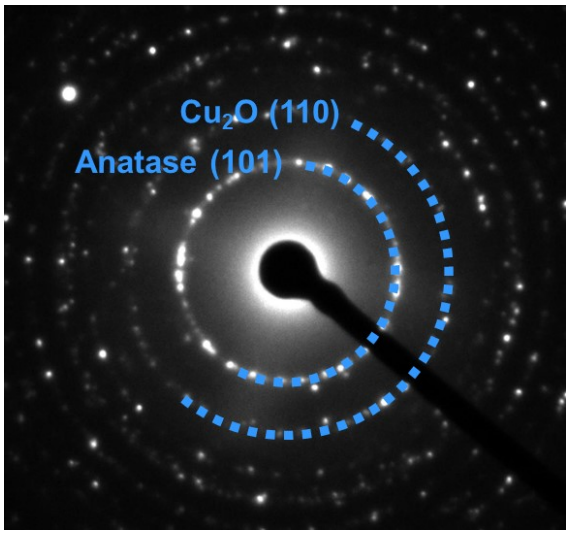

Fig. S1 The image of the selected area electron diffraction about T-N-Cu1.5 sample.

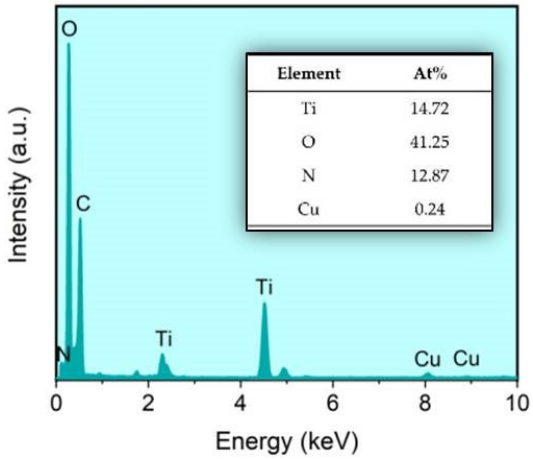

Fig. S2 EDS analysis of T-N-Cu1.5 sample.

Table S1. ICP-OES patterns of T-N-Cu1.5 sample.

Element	**Cu (Wt%)**
T-N-Cu1.5	0.95%

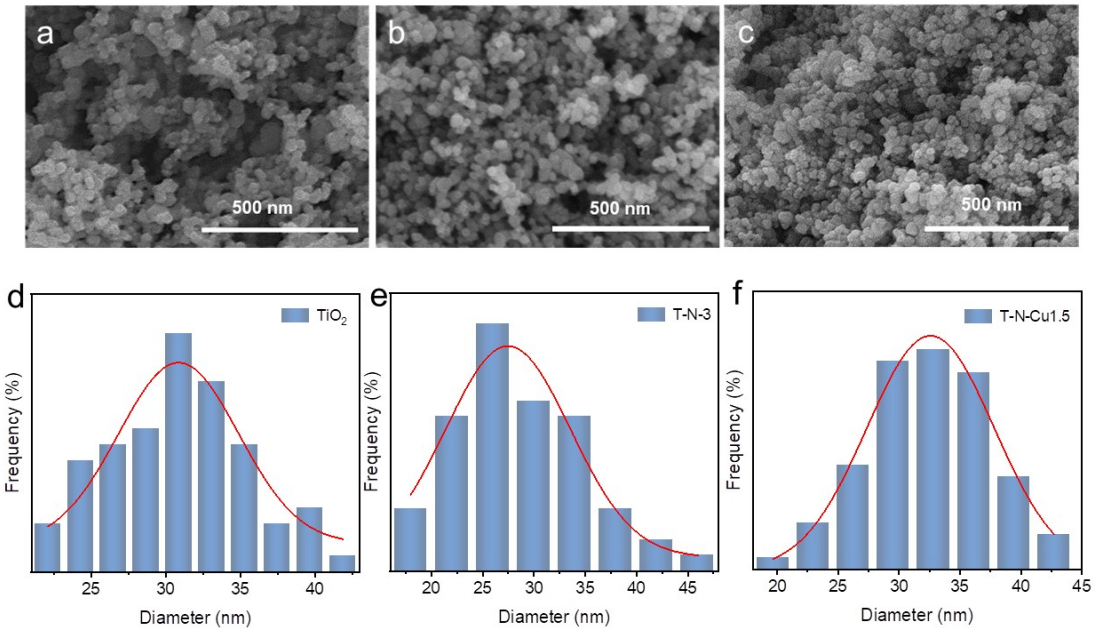

Fig. S3 SEM images and particle size distribution results of TiO_2, T-N and T-N-Cu1.5% samples.

Table S2. Average diameter data of **TiO_2, T-N and T-N-Cu1.5% samples.**

Sample	TiO_2	T-N	T-N-Cu1.5
Average diameter (nm)	30.96	29.43	32.83

The particle size of the sample was analyzed, and the results were shown in Table S2 and Fig. S3. The analysis revealed that there was almost no change in particle size of the substrate TiO_2 after incorporating Cu_2O QDs.

The images in Fig. S3 and Table S2 revealed that the deposition of Cu_2O QDs and subsequent adsorption of hydrazine hydrate did not result in significant morphological changes, with the original homogeneous particle shape remaining unchanged. Particle size analysis data indicated that the particle sizes of the three specimens were 30.96 nm, 29.43 nm, and 32.83 nm, respectively.

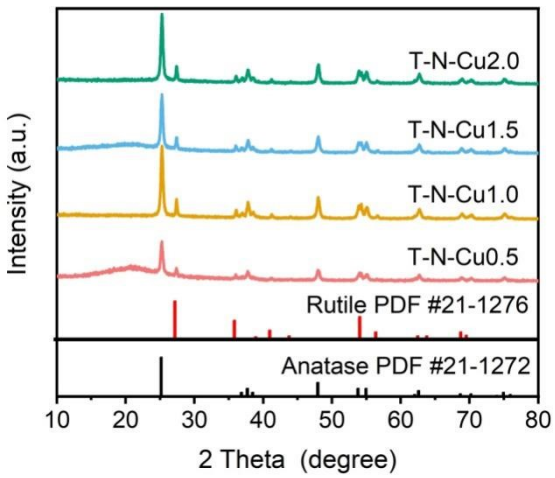

Fig. S4 XRD patterns of TiO_2 and T-N-Cu (0.5%, 1%, 1.5%, 2%) samples.

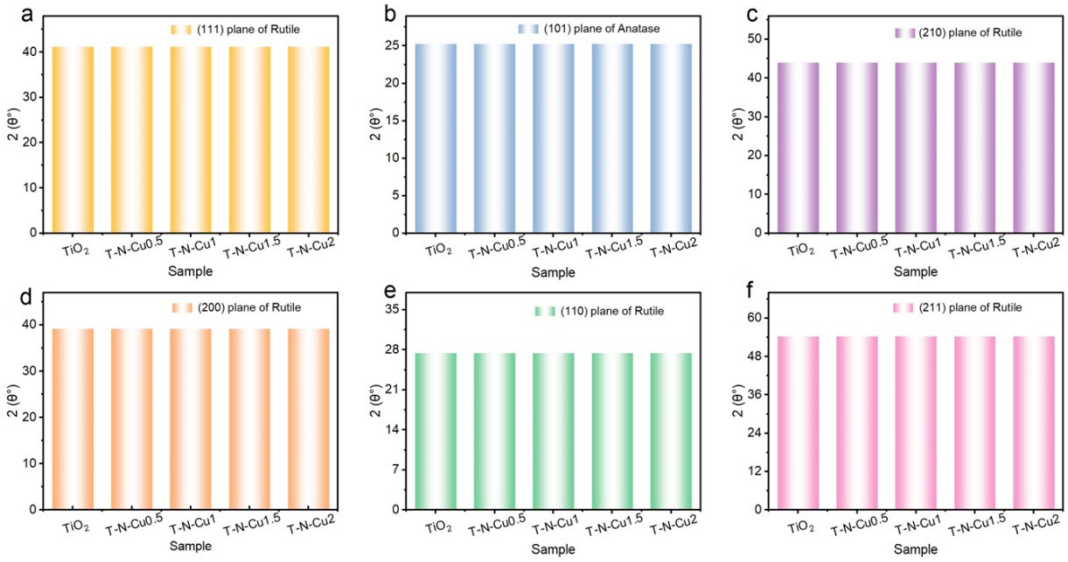

Fig. S5 The peak position of each sample in XRD: (a) (111) plane of rutile, (b) (101) plane of anatase, (c) (210) plane of rutile, (d) (200) plane of rutile, (e) (110) plane of rutile, (f) (211) plane of rutile.

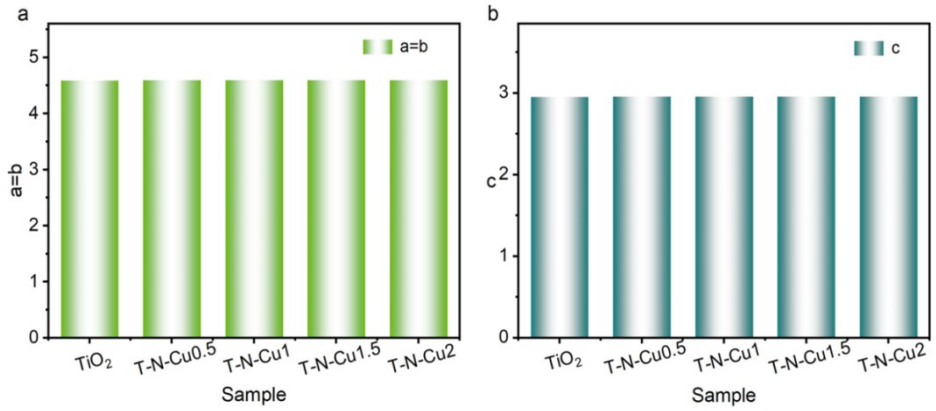

Fig. S6 The calculated lattice constant of each sample from XRD.

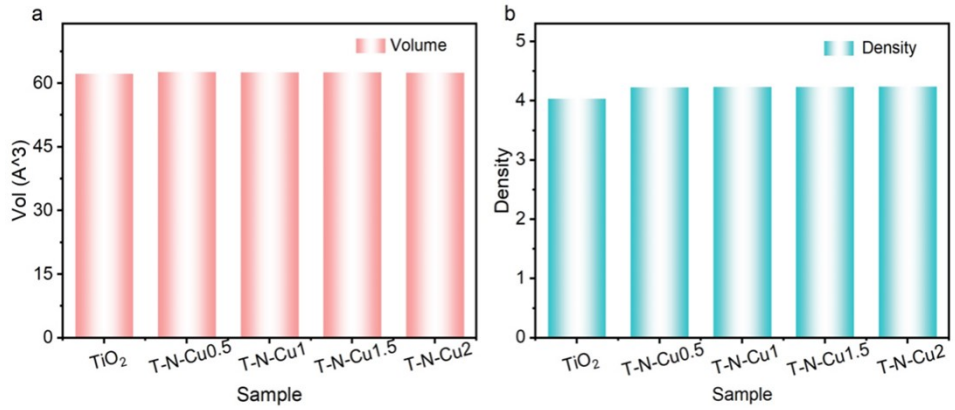

Fig. S7 The calculated lattice volume and density of as-obtained sample from XRD.

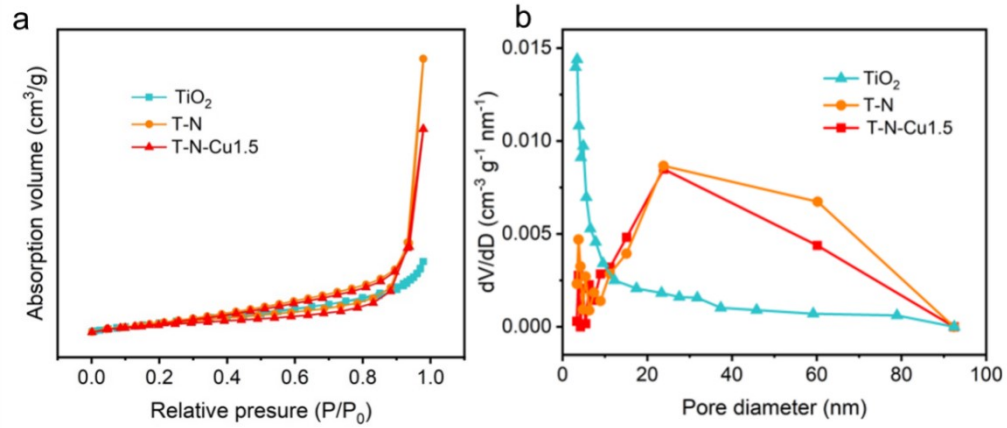

Fig. S8 (a) N_2 adsorption-desorption isotherms, (b) pore-size distribution curves of **TiO_2, T-N and T-N-Cu1.5% samples.**

Table S3 Surface area, pore diameter and pore volume of **TiO_2, T-N and T-N-Cu1.5 samples.**

Sample	Surface area (m^2/g)	Pore diameter (cm^3/g)	Pore volume (nm)
TiO_2	53.2	3.4	0.14
T-N	62.6	23.8	0.56
T-N-Cu1.5	51.9	23.8	0.4

The nitrogen adsorption–desorption procedure was systematically employed to characterize the mesoporous structure of the catalysts. As displayed in Fig. S8, the TiO_2, T-N and T-N-Cu1.5 samples all manifested a type IV adsorption-desorption curve, featuring a discernible loop that attested to the presence of mesoporous structure. The elucidation of pore size distribution and pore volume of the catalysts were accomplished by the application of the Brunauer-Emmett-Teller (BET) and Barret-Joyner-Halenda (BJH) methods. Upon careful comparison of Table S3 and Fig. S9b, it can be seen that there are minimal changes in specific surface area, pore diameter, and pore volume for the three specimens. The adsorption of hydrazine hydrate and the incorporation of Cu_2O QDs co-catalysts have no significant impact on the specific surface area, pore size and pore volume of TiO_2. This observation lends further support to the notion that these specific structural characteristics of specific surface area, pore size distribution, and pore volume do not play a decisive role in modulating the energy band structure.

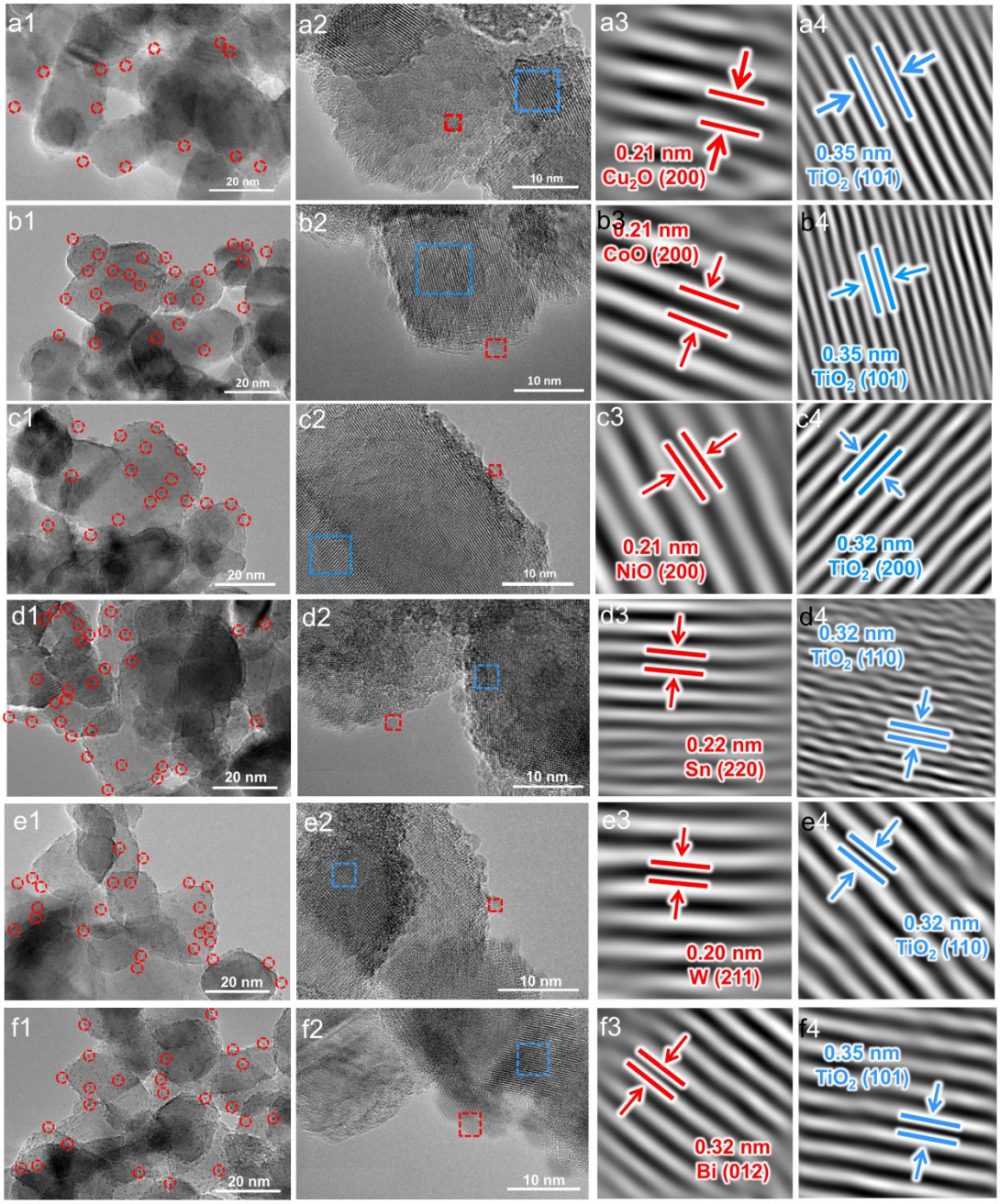

Fig. S9 (a1,a2) TEM and HR-TEM images, (a3,a4) lattice spacing of T-N-Cu1.5 sample. (b1,b2) TEM and HR-TEM images, (b3,b4) lattice spacing of T-N-Co1.5 sample. (c1,c2) TEM and HR-TEM images, (c3,c4) lattice spacing of T-N-Ni1.5 sample. (d1,d2) TEM and HR-TEM images, (d3,d4) lattice spacing of T-N-Sn1.5 sample. (e1,e2) TEM and HR-TEM images, (e3,e4) lattice spacing of T-N-W1.5 sample. (f1,f2) TEM and HR-TEM images, (f3,f4) lattice spacing of T-N-Bi1.5 sample.

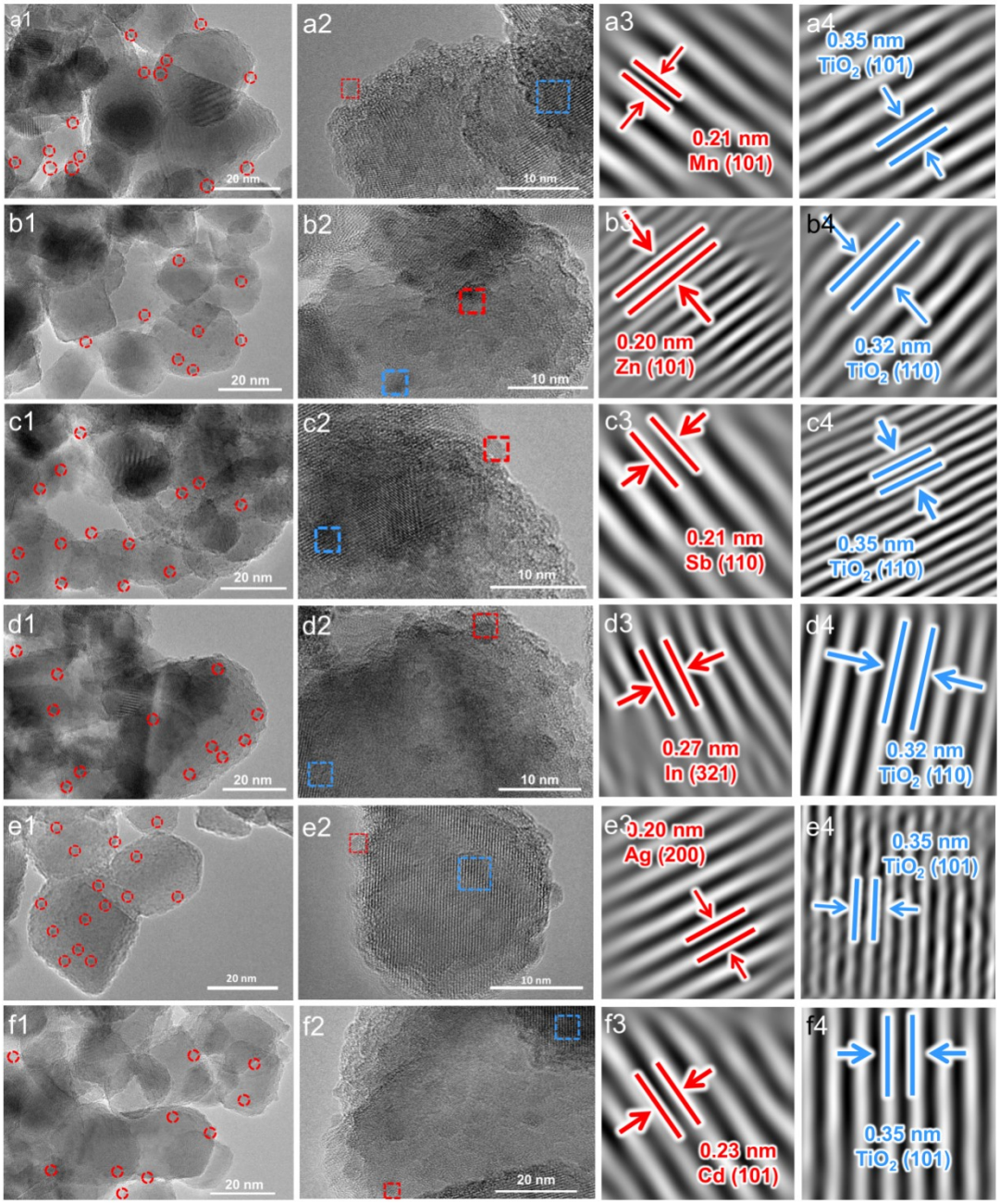

Fig. S10 (a1,a2) TEM and HR-TEM images, (a3,a4) lattice spacing of T-N-Mn1.5 sample. (b1,b2) TEM and HR-TEM images, (b3,b4) lattice spacing of T-N-Zn1.5 sample. (c1,c2) TEM and HR-TEM images, (c3,c4) lattice spacing of T-N-Bi1.5 sample. (d1,d2) TEM and HR-TEM images, (d3,d4) lattice spacing of T-N-In1.5 sample. (e1,e2) TEM and HR-TEM images, (e3,e4) lattice spacing of T-N-Ag1.5 sample. (f1,f2) TEM and HR-TEM images, (f3,f4) lattice spacing of T-N-Cd1.5 sample.

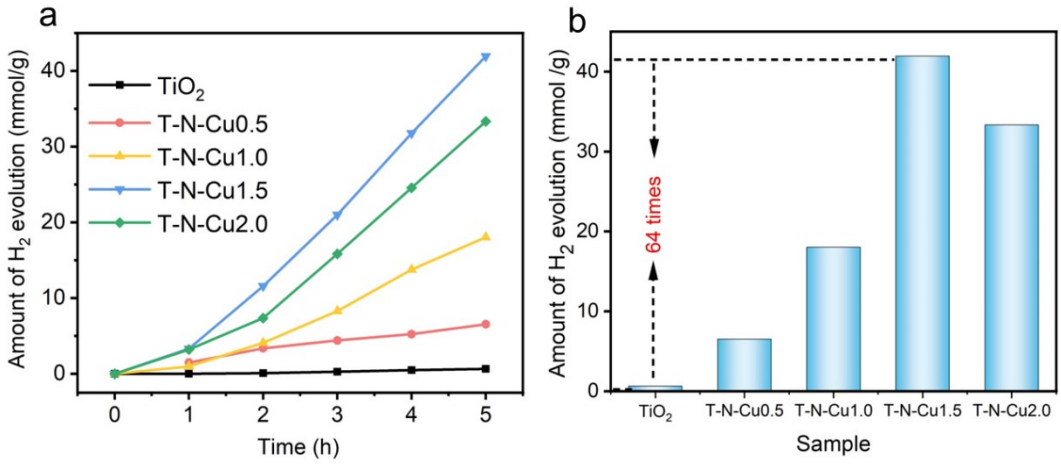

Fig. S11 Comparison the amount of photocatalytic hydrogen evolution of TiO_2 and T-N-Cu (0.5%, 1%, 1.5%, 2%) samples.

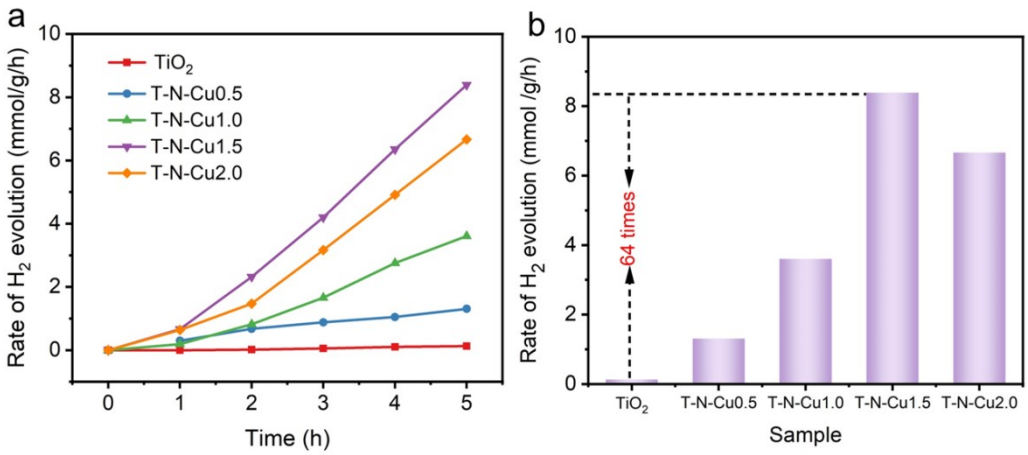

Fig. S12 Comparison the rate of photocatalytic hydrogen evolution of TiO_2 and T-N-Cu (0.5%, 1%, 1.5%, 2%) samples.

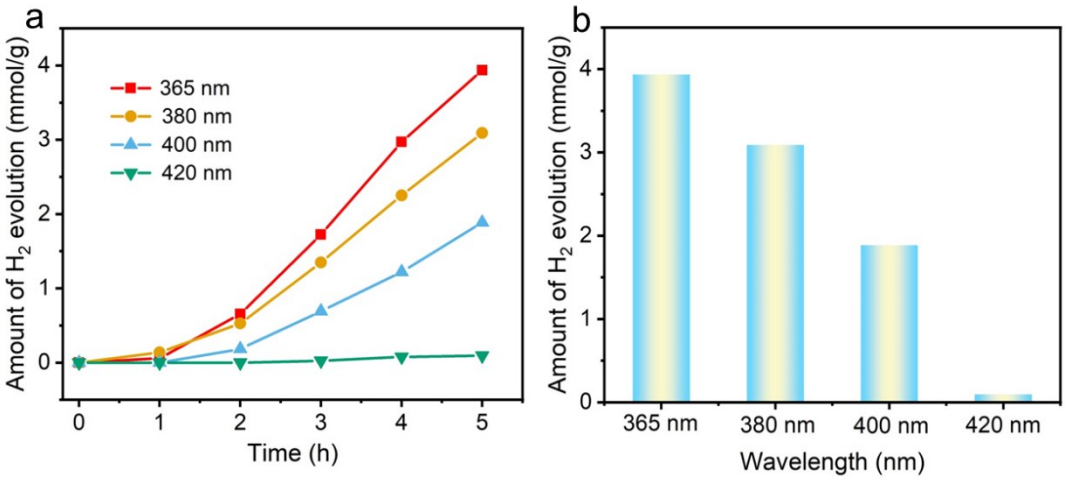

Fig. S13 Comparison the amount of photocatalytic hydrogen evolution of TiO_2 and T-N-Cu1.5 samples under different wavelength of light irradiation.

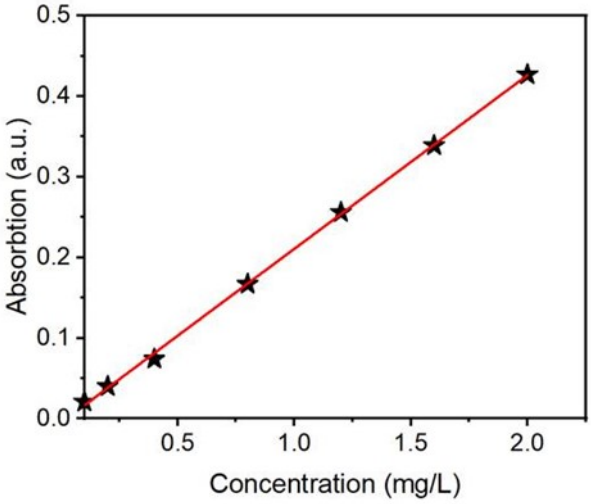

Fig. S14 Standard curve of NH_4^+ detection by Nessler's reagent colorimetric method.

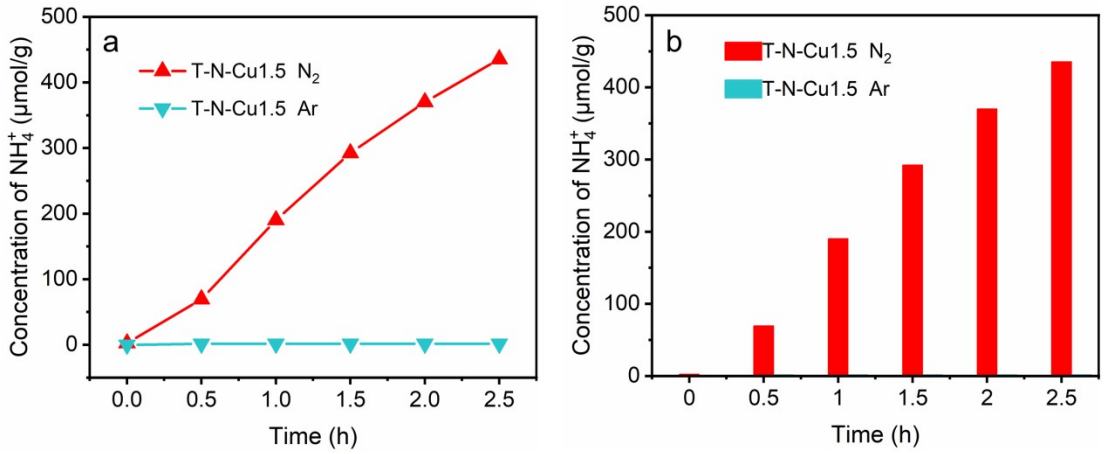

Fig. S15 Photocatalytic nitrogen fixation of T-N-Cu1.5 samples under different atmospheres

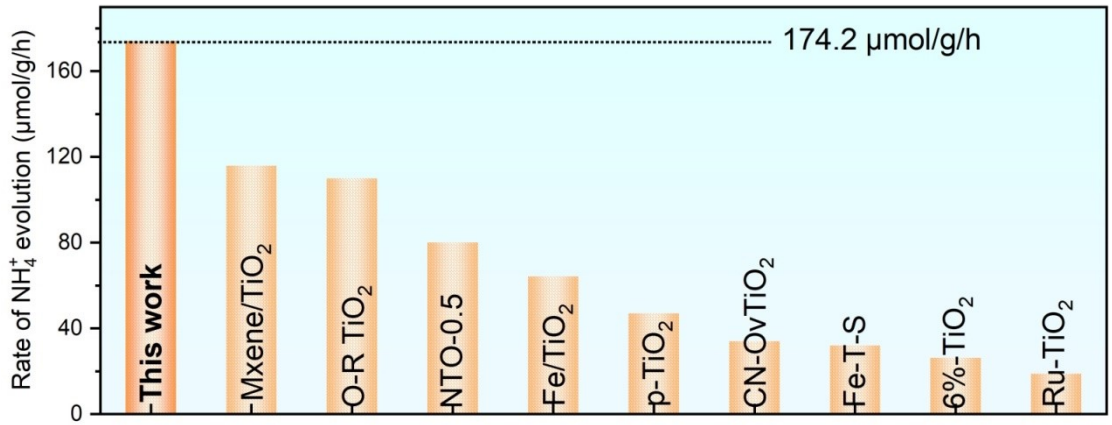

Fig. S16 Comparison rate of NH_4^+ evolution with recently reported superior TiO_2-based catalysis [1-9].

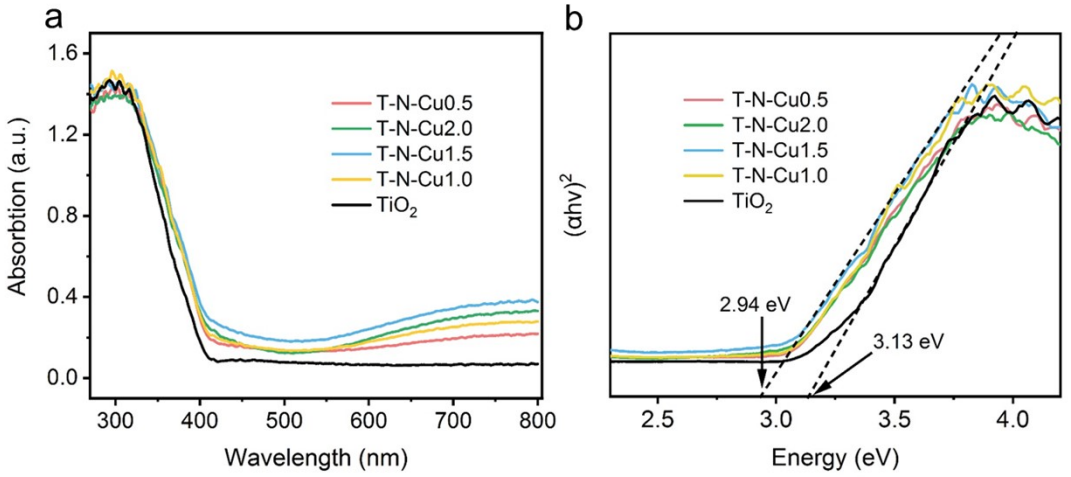

Fig. S17 Comparison of UV-vis absorption and corresponding Tauc plot of TiO_2 and T-N-Cu (0.5%, 1%, 1.5%, 2%) samples.

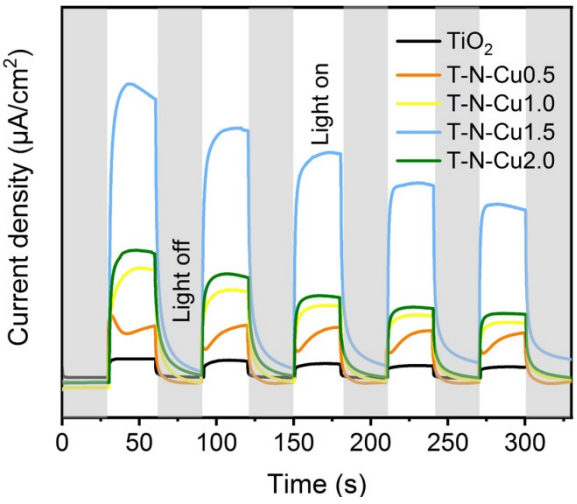

Fig. S18 Transient photocurrent density versus time (I-T) curve of **T-N-Cu (0.5%, 1%, 1.5%, 2%) samples.**

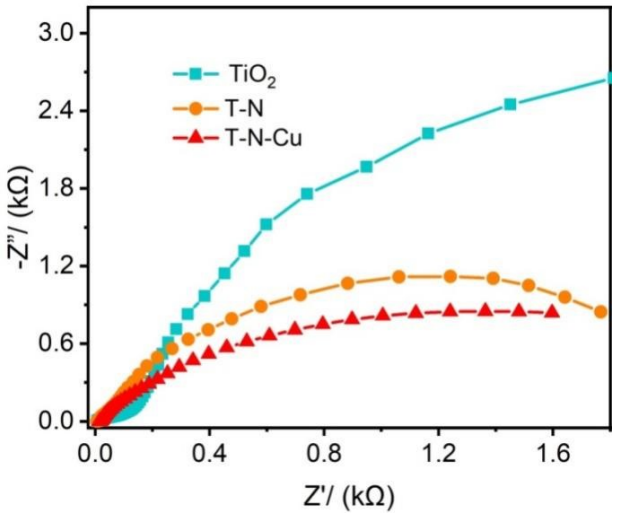

Fig. S19 EIS curves of TiO_2, T-N and T-N-Cu1.5 samples under lighting condition.

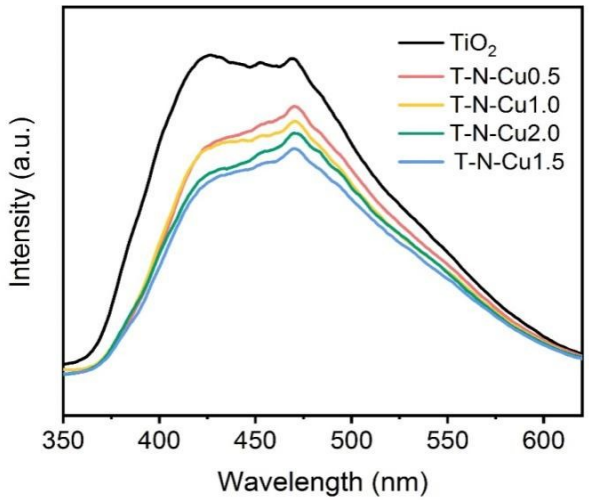

Fig. S20 Photoluminescence spectra of TiO_2 and T-N-Cu (0.5%, 1%, 1.5%, 2%) samples.

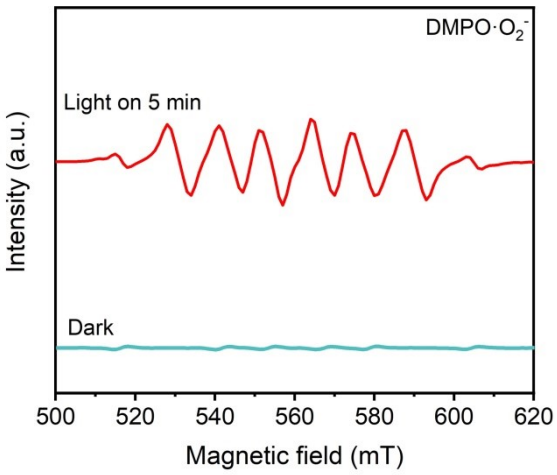

Fig. S21 DMPO- •O_2^- EPR response of T-N-Cu sample before and after visible light irradiation.

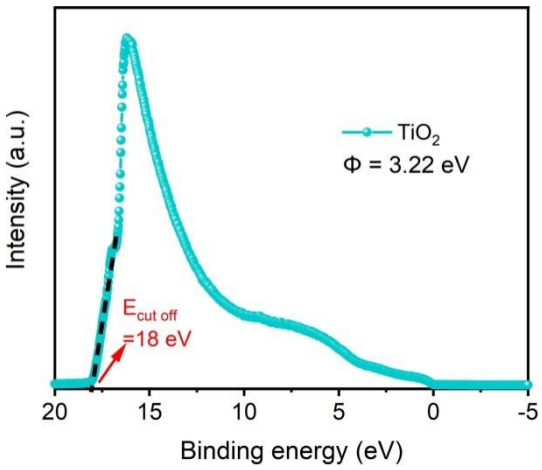

Fig. S22 Ultraviolet electron spectra (UPS) of TiO_2.

References

1 G. M. Ren, M. Shi, S. T. Liu, Z. Z. Li, Z. S. Zhang, X. C. Meng, Chem. Eng. J. 2023, **454**, 140158-140167.

2 Y. X. Zhao, Y. F. Zhao, R. Shi, B. Wang, G. I. N. Waterhouse, L. Z. Wu, C. H. Tung, T. R. Zhang, Adv. Mater. 2019, **31**, 1806482-1806490.

3 W. Gao, X. Li, S. Luo, Z. Luo, X. Zhang, R. Huang, M. Luo, J. Colloid Interf. Sci. 2021, **585**, 20-29.

4 Q. Y. Liu, H. D. Wang, R. Tang, Q. Cheng, Y. J. Yuan, ACS Appl. Nano Mater. 2021, **4**, 8674-8679.

5 C. Li, M. Z. Gu, M. M. Gao, K. N. Liu, X. Y. Zhao, N. W. Cao, J. Feng, Y. M. Ren, T. Wei, Z. M. Yi, J. Colloid Interf. Sci. 2022, **609**, 341-352.

6 Y. Bo, H. Wang, Y. Lin, T. Yang, R. Ye, Y. Li, C. Hu, P. Du, Y. Hu, Z. Liu, R. Long, C. Gao, B. Ye, L. Song, X. Wu, Y. Xiong, Angew. Chem. Int. Ed. 2021, **60**, 16085-16092.

7 W. Ding, X. Li, S. Su, Z. Liu, Y. Cao, L. Meng, S. Yuan, W. Wei, M. Luo, Nanoscale 2023, **15**, 4014-4021.

8 S. Wu, C. He, L. Wang, J. Zhang, Chem. Eng. J. 2022, **443**, 136425-136433.

9 S. Wu, Z. Chen, W. Yue, S. Mine, T. Toyao, M. Matsuoka, X. Xi, L. Wang, J. Zhang, ACS Catal. 2021, **11**, 4362-4371.